Journal of the Taiwan Institute of Chemical Engineers 42 (2011) 186–189

Contents lists available at ScienceDirect

Journal of the Taiwan Institute of Chemical Engineers

journal homepage: www.elsevier.com/locate/jtice

Structural effects on magnetic property of reciprocal opalline structures of iron–nickel alloys prepared with template-assisted electrodeposition

Cheng-Yu Kuo, Kung-Hsun Huang, Shih-Yuan Lu *

Department of Chemical Engineering, National Tsing-Hua University, Hsinchu 30013, Taiwan

ARTICLE INFO

Article history:
Received 5 January 2010
Accepted 5 May 2010

Keywords:
Photonic crystal
Double template
Nickel–iron alloy
Coercivity
Opal
Inverse opal

ABSTRACT

Reciprocal opalline structures, opals and corresponding inverse opals, of iron–nickel alloys ($FeNi_3$) were successfully fabricated with template-assisted electrodeposition processes. The magnetic properties of the structures were studied against the structural features, including shape and characteristic length, of these reciprocal opals. The magnetic $FeNi_3$ opals and corresponding inverse opals were obtained from starting polystyrene opals via a double and single templating procedure, respectively. The structural feature sizes of the opal and corresponding inverse opal were adjusted with the diameter of the starting PS spheres, from 250 to 440 nm. The coercive fields of the inverse opals were found much larger than those of the corresponding opals, attributable to the strong local shape anisotropy and intersections of the thin backbone of the inverse opal. The coercive fields increased with decreasing structural feature size, because of the increase in the densities of domain wall pinning sites and domain vortex sites caused by the feature size reduction. The present work demonstrated the drastic effects of shape and characteristic length on the coercive fields of reciprocal structures.

1. Introduction

Nanostructured magnetic materials have drawn much research attention in the past decade because of the wide range potential applications in sensor (O'Barr *et al.*, 1997; Schneider *et al.*, 2001; Wu *et al.*, 2006), magnetic storage (Duvail *et al.*, 1998; Wassermann *et al.*, 1998), and magnetoelectronic devices (Bal *et al.*, 2002; Bibes *et al.*, 2002; Xi and Shi, 2004). For such materials, the structure and feature size have profound influences on their magnetic properties because of the strong magnetic interactions bound to occur within the structure. Consequently, the precise structure control of magnetic materials becomes a challenging issue and has drawn much research attention in recent years. A wide range of approaches have been developed to prepare controllable nanostructured materials of unusual magnetic properties, such as ultrathin films (Chang *et al.*, 2007; Li and Wang, 2000; Xu *et al.*, 1998; Zhao *et al.*, 2006), nanowire arrays (Cagnon *et al.*, 2007; Huang *et al.*, 2002; Liang *et al.*, 2005; Zhang *et al.*, 2003; Zheng *et al.*, 2000), multilayer films (Ghosh *et al.*, 2006; Kirk *et al.*, 2002; Liu *et al.*, 2005), and macroporous structures (Eagleton and Searson, 2004; Galloro *et al.*, 2002). Among the many approaches, colloidal template-assisted electrochemical depositions have gained popularity for creation of macroporous structures because of their simplicity and cost effectiveness. Furthermore, the resulting macroporous structures belong to a class of photonic crystals, termed synthetic opals and inverse opals, and may possess additional functioning properties (Kahi and Grishin, 2004; Wang and Fan, 2005).

Photonic crystals are a special class of composite structure possessing periodic variation in dielectric contrast. Such structures exhibit the unusual optical phenomenon of photonic bandgap, from which applications in advanced optical and sensing devices such as waveguide (Kuo and Lu, 2007), superprism (Kosaka *et al.*, 1998), microcavity (Foresi *et al.*, 1997), filter (Fan *et al.*, 1998), and chemical sensor (Kuo *et al.*, 2007) have been developed. Magnetic opals and inverse opals thus may possess multiple functionalities for novel applications combining/coupling magnetic and optical properties.

In this article, the opal and corresponding inverse opal of $FeNi_3$ were successfully fabricated with electrodeposition from starting polystyrene (PS) opals via a double and single templating procedure, respectively (Kuo and Lu, 2008a,b). With such structures available, one can study the variations in magnetic property of reciprocal structures caused by the fundamental differences in their structural features. Here, $FeNi_3$ is one of the permalloys ($Fe_{100-x}Ni_x$, $x = 35–82$), which are soft magnetic materials with negligible magnetostriction and magnetocrystalline anisotropies. With this model material, one can rule out the possible contributions to the magnetic variations resulting from the magnetostriction and magnetocrystalline anisotropy effects. The in-plane (with the externally applied magnetic field parallel to the substrate) coercive fields of the reciprocal opalline structures

* Corresponding author. Tel.: +886 3 5714364; fax: +886 3 5715408.
E-mail address: sylu@mx.nthu.edu.tw (S.-Y. Lu).

1876-1070/$ – see front matter © 2010 Taiwan Institute of Chemical Engineers. Published by Elsevier B.V. All rights reserved.
doi:10.1016/j.jtice.2010.05.004

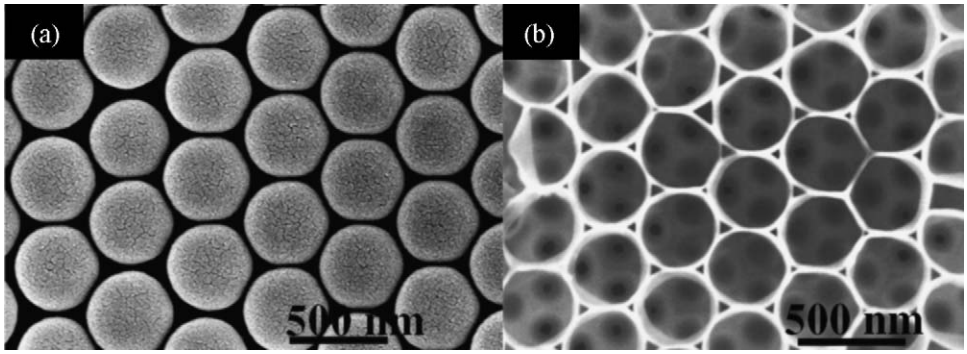

Fig. 1. Top view SEM images of (a) the PS opal template and (b) polypyrrole inverse opal template.

of $FeNi_3$ were found to vary drastically subject to variations in structure and feature size.

2. Experimental

Uniform sized PS spheres were prepared using an emulsifier-free emulsion polymerization process (Im *et al.*, 2002), with the sphere diameter adjusted by the amount of co-monomer addition. Typically, 0.01 g co-monomer of sodium styrene sulfonate and 0.25 g buffer of sodium bicarbonate were added into 450 g deionized water at 75 °C. After stirring for 10 min, 50 g styrene monomer was introduced into the solution and the mixture was further stirred for 2 h. The polymerization reaction was initiated by introducing 0.25 g initiator of potassium persulfate into the solution and the polymerization proceeded for 24 h. The resulting PS spheres were with a diameter of 440 nm. To obtain PS spheres with diameters of 250, 320, and 400 nm, 0.1, 0.04, and 0.02 g of co-monomer were used, respectively.

Slide glass, coated with 10 nm of adhesion-promoting chromium layer followed by 100 nm of gold layer as the conductive layer by thermal evaporation under vacuum at a depositing rate of 1 Å/s, was used as the deposition substrate. The starting PS opals were obtained with a vaporization-assisted vertical deposition process (Jiang *et al.*, 1999). Typically, the deposition substrate was immersed vertically into an ethanolic PS suspension of 1.5 wt% at 25 °C and let still for PS opal formation. With evaporation of ethanol, the liquid level dropped slowly and the PS spheres self-assembled into an fcc array, forming the PS opal, on the slowly exposing substrate surface.

The resulting PS opals, in addition to serving as a template for creation of the $FeNi_3$ inverse opals, were also used as a template to construct polypyrrole inverse opals, later used for fabrication of the $FeNi_3$ opals, by infiltrating polypyrrole into the void space of the PS opals through electrodeposition, followed by solvent etching removal of the PS template. The electrodeposition of polypyrrole was carried out in a three-electrode cell using Pt as the counter electrode and a saturated calomel electrode (SCE) as the reference electrode. The deposition was operated at 0.6 V (versus SCE) in the electrolyte of 0.04 M NaCl and 0.2 M pyrrole aqueous solution. The solvent etching was achieved with immersion in tetrahydrofuran (THF) at 60 °C for 1 h twice. The resulting polypyrrole inverse opal template was baked at 200 °C for 2 h to reduce the conductivity of the polypyrrole backbone to enable a bottom-up electrodeposition growth of $FeNi_3$ in the following step. The electrodeposition of $FeNi_3$ into the PS opals and polypyrrole inverse opals, for completion of the $FeNi_3$ opal and inverse opal fabrication, respectively, was carried out at −1.2 V (versus SCE) in an aqueous electrolyte composed of 21 g/L $NiSO_4$, 5.6 g/L $FeSO_4$, 6.2 g/L H_3BO_3, and 1.4 g/L sodium dodecyl sulfate (SDS) at pH 2.5 adjusted by H_2SO_4. Note that because of the well know abnormal codeposition phenomenon commonly encountered in codeposition of metallic species, more than stoichiometrically necessary Ni source was used. The addition of SDS helped the penetration of aqueous electrolytes into the narrow void space afforded by the hydrophobic PS opals or polypyrrole inverse opals.

Field emission scanning electron microscope (FE-SEM) images were obtained on a JEOL JSM-6700 microscope operated at 3 kV. XRD spectra were recorded on MAC Science, MXP18 (X-ray diffractometer, λ = 1.54056 Å). The in-plane coercive fields were measured with a vibrating sample magnetometer (VSM).

3. Results and discussion

Fig. 1 shows the typical top-view SEM images of the PS opal and polypyrrole inverse opal, constructed from starting PS spheres of 440 nm, which were the direct templates used to create the $FeNi_3$ inverse opal and opal, respectively. The hexagonal arrangements of the PS spheres and air spheres of the images revealed the (1 1 1) growth plane of the fcc structure. Evidently, the two structures are reciprocal to each other and possess dramatically different

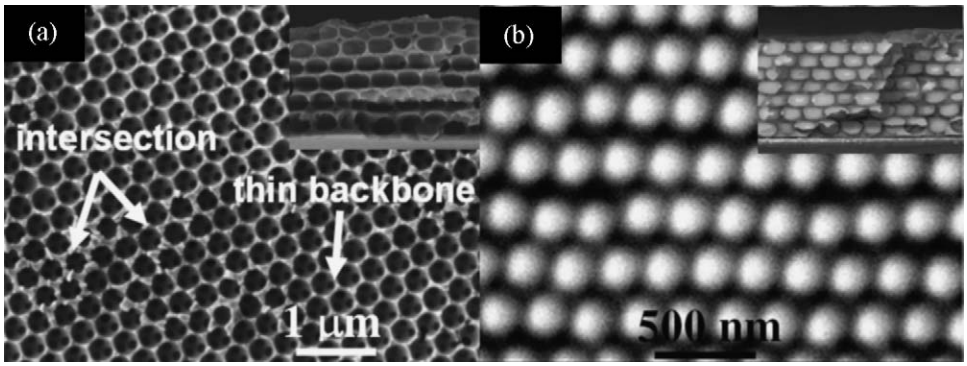

Fig. 2. Top view SEM images of the resultant $FeNi_3$ (a) inverse opal and (b) opal, with the corresponding cross-sectional SEM images shown in the insets.

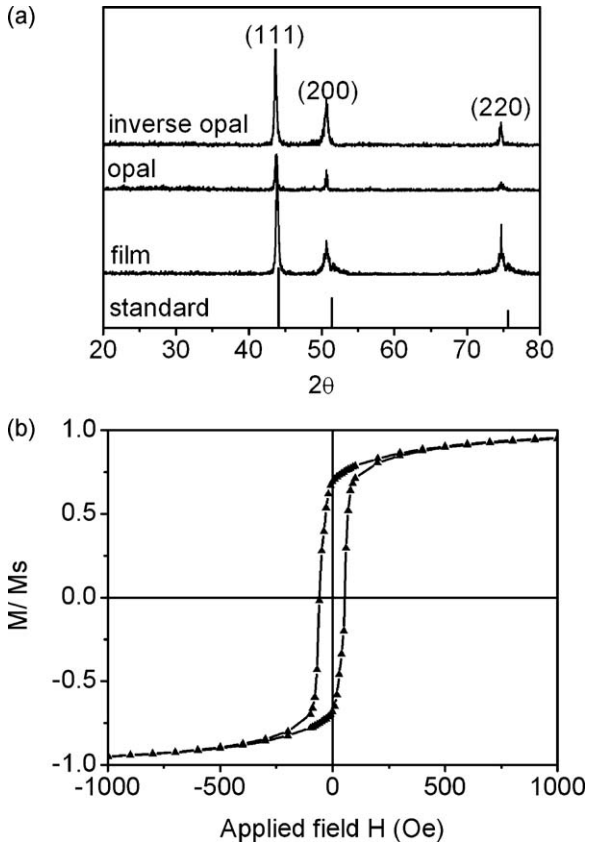

Fig. 3. (a) XRD patterns of the $FeNi_3$ opal, inverse opal, and film. (b) A typical hysteresis loop obtained from a $FeNi_3$ inverse opal with the applied field parallel to the substrate plane.

structural characteristics. The opal structure is composed of regularly arranged material spheres at point contacts and has a characteristic length scale of the diameter of the constituent spheres, whereas the inverse opal structure is a highly porous network with regularly arranged air spheres embedded and takes the thickness of the thin backbone as the primary characteristic length scale. Furthermore, there are formed a high density of intersections of the thin backbones in the inverse opal structure. These structural differences caused drastic differences in in-plane coercive fields for reciprocal magnetic opals and inverse opals.

Fig. 2 shows the typical top-view SEM images for the fabricated $FeNi_3$ opal and inverse opal, with the corresponding cross-sectional SEM images shown as the insets. Note that when preparing the samples for the cross-sectional SEM images, the samples had to be cut to create cleavages for SEM imaging, and the compression force applied to the samples distorted the structures and thus the constituent PS spheres and air spheres of the $FeNi_3$ opal and inverse opal, respectively, appeared elongated in the plane direction.

The crystalline phase of the iron–nickel alloy was identified with the XRD patterns. For comparison purposes, iron–nickel alloy thin films deposited on a gold coated slide glass were also prepared with the same electrodeposition conditions. The XRD patterns, Fig. 3(a), show that pure $FeNi_3$ of cubic phase (JCPDs No. 65-3244) was obtained for the opal, inverse opal, and thin film samples.

The in-plane coercive fields of the $FeNi_3$ opals and inverse opals as a function of the diameter of the starting PS spheres were tabulated in Table 1. Also included is the coercive field for the $FeNi_3$ film for comparison. Fig. 3(b) shows a typical hysteresis loop of the sample with the applied magnetic field pointed parallel to the

Table 1
In-plane coercive fields (Oe) of $FeNi_3$ opals and inverse opals as a function of starting PS sphere size.

Structure	Diameter (nm)			
	250	320	400	440
Opal	21	14	9.5	6.6
Inverse opal	165	111	81	57
Film		6		

substrate plane. Several points can be observed from the table. First, at the same PS sphere diameter, the in-plane coercive fields of the inverse opals were much larger than those of the corresponding opals. As already identified that the compositions and crystalline phases of the iron–nickel alloys deposited in the $FeNi_3$ opal, inverse opal, and film were the same, the drastic differences in in-plane coercive fields most likely came from the structural characteristics of the samples. For the opals, the primary characteristic length is the diameter of the constituent spheres, in the order of several hundreds of nanometers, whereas for the inverse opals the primary characteristic length is the width of the thin backbone, around several tens of nanometers. Evidently, there existed about one order of magnitude difference in characteristic length. More importantly, such differences in characteristic length were accompanied by the strong shape anisotropy of the thin backbone of the inverse opal. The thin backbones make it difficult for the magnetic domains to rotate when subject to externally applied magnetic fields, leading to larger coercive fields (Barnard *et al.*, 1996; Eagleton and Searson, 2004). The narrow space of the thin backbone also promoted domain wall pinning, again resulting in larger coercive fields. Furthermore, the intersections of these thin backbones served as the sites for possible magnetic domain vortices, further favoring larger coercive fields (Bartlett *et al.*, 2003). In contrast to the situation encountered in inverse opals, smaller void fractions and larger Ni_3Fe structural feature sizes were associated with the Ni_3Fe opals. Both factors decrease the contribution of the locking effect to the coercive fields. Consequently, significant increases in coercive field, about 8-fold, were observed for the inverse opals as compared with the corresponding opals.

Second, the coercive fields of both the $FeNi_3$ opals and inverse opals increased with decreasing diameter of the material and air sphere, respectively. As the diameter of the sphere, material or air, decreases, the densities of surface areas and thus the domain wall pinning sites and domain vortex sites increase (Ross *et al.*, 2002; Wegrowe *et al.*, 1999), leading to enhanced coercive fields. For opals, the increase in sphere diameter makes the opal structure appear and behave more like a bulk structure. At the sphere diameter of 440 nm, the in-plane coercive field of the $FeNi_3$ opal was almost the same with that of the $FeNi_3$ film.

4. Conclusion

$FeNi_3$ opals and corresponding inverse opals were successfully fabricated with a single and double template-assisted electrodeposition processes, respectively. The two reciprocal opalline structures exhibited drastically different magnetic properties, attributable to the differences in structural characteristics. The thin backbones and the intersections of which of the inverse opals gave rise to much enhanced coercive fields for the inverse opals as compared to the corresponding opals. The decrease in sphere diameter increased the densities of surface areas and thus domain wall pinning sites and domain vortex sites, leading to larger coercive fields.

Acknowledgments

The authors thank the National Science Council of the Republic of China (Taiwan) under grant NSC 98-2221-E-007-036-MY3 and the Top program of the National Tsing-Hua University for financial support.

References

Bal, M., A. Ursache, M. T. Tuominen, J. T. Goldbach, and T. P. Russell, "Nanofabrication of Integrated Magnetoelectronic Devices Using Patterned Self-assembled Copolymer Templates," *Appl. Phys. Lett.*, **81**, 3479 (2002).

Barnard, J. A., H. Fujiwara, V. R. Inturi, J. D. Jarratt, T. W. Scharr, and J. L. Weston, "Nanostructured Magnetic Networks," *Appl. Phys. Lett.*, **69**, 2758 (1996).

Bartlett, P. N., M. A. Ghanem, I. S. E. Hallag, P. de Groot, and A. Zhukov, "Electrochemical Deposition of Macroporous Magnetic Networks Using Colloidal Templates," *J. Mater. Chem.*, **13**, 2596 (2003).

Bibes, M., S. Valencia, L. Balcells, B. Martínez, J. Fontcuberta, M. Wojcik, S. Nadolski, and E. Jedryka, "Charge Trapping in Optimally Doped Epitaxial Manganite Thin Films," *Phys. Rev. B*, **66**, 134416 (2002).

Cagnon, L., Y. Dahmane, J. Voiron, S. Pairis, M. Bacia, L. Ortega, N. Benbrahim, and A. Kadri, "Electrodeposited CoPt and FePt Alloys Nanowires," *J. Magn. Magn. Mater.*, **310**, 2428 (2007).

Chang, H. W., J. S. Tsay, Y. L. Chiou, K. T. Huang, W. Y. Chan, and Y. D. Yao, "Coercivity Enhancement of Ultrathin Co/Ge(1 1 1) Films by Co/O Interfacial Anisotropy," *J. Magn. Magn. Mater.*, **310**, E741 (2007).

Duvail, J. L., S. Dubois, L. Piraux, A. Vaures, A. Fert, D. Adam, M. Champagne, F. Rousseaux, and D. Decanini, "Electrodeposition of Patterned Magnetic Nanostructures," *J. Appl. Phys.*, **84**, 6359 (1998).

Eagleton, T. S. and P. C. Searson, "Electrochemical Synthesis of 3D Ordered Ferromagnetic Nickel Replicas Using Self-Assembled Colloidal Crystal Templates," *Chem. Mater.*, **16**, 5027 (2004).

Fan, S. H., P. R. Villeneuve, J. D. Joannopoulos, and H. A. Haus, "Channel Drop Filters in Photonic Crystals," *Opt. Express*, **3**, 4 (1998).

Foresi, J. S., P. R. Villeneuve, J. Ferrera, E. R. Thoen, G. Steinmeyer, S. H. Fan, J. D. Joannopoulos, L. C. Kimerling, H. I. Smith, and E. P. Ippen, "Photonic-bandgap Microcavities in Optical Waveguides," *Nature*, **390**, 143 (1997).

Galloro, J., M. Ginzburg, H. Miguez, S. M. Yang, N. Coombs, A. S. Sefat, J. E. Greedan, I. Manner, and G. A. Ozin, "Replicating the Structure of a Crosslinked Polyferrocenylsilane Inverse Opal in the Form of a Magnetic Ceramic," *Adv. Func. Mater.*, **12**, 382 (2002).

Ghosh, S. K., A. K. Grover, P. Chowdhury, S. K. Gupta, G. Ravikumar, D. K. Aswal, M. S. Jumar, and R. O. Dusane, "High Magnetoresistance and Low Coercivity in Electrodeposited Co/Cu Granular Multilayers," *Appl. Phys. Lett.*, **89**, 132507 (2006).

Huang, Y. H., H. Okumura, and G. C. Hadjipanayis, "CoPt and FePt Nanowires by Electrodeposition," *J. Appl. Phys.*, **91**, 6869 (2002).

Im, S. H., Y. T. Lim, D. J. Suh, and O. O. Park, "Three-dimensional Self-assembly of Colloids at a Water–Air Interface—A Novel Technique for the Fabrication of Photonic Bandgap Crystals," *Adv. Mater.*, **14**, 1367 (2002).

Jiang, P., J. F. Bertone, K. S. Hwang, and V. L. Colvin, "Single-crystal Colloidal Multilayers of Controlled Thickness," *Chem. Mater.*, **11**, 2132 (1999).

Kahi, S. and M. Grishin, "Enhanced Faraday Rotation in All-garnet Magneto-optical Photonic Crystal," *Appl. Phys. Lett.*, **84**, 1438 (2004).

Kirk, T. L., O. Hellwig, and E. E. Fullerton, "Coercivity Mechanisms in Positive Exchange-biased Co Films and Co/Pt Multilayers," *Phys. Rev. B*, **65**, 224426 (2002).

Kosaka, H., T. Kawashima, A. Tomita, M. Notomi, T. Tamamura, T. Sato, and S. Kawakami, "Superprism Phenomena in Photonic Crystals," *Phys. Rev. B*, **58**, 10096 (1998).

Kuo, C. Y. and S. Y. Lu, "Fabrication of Patterned Inverse Opal Structure through Physical Confinement Assembly and Selective Electrochemical Deposition," *J. Am. Ceram. Soc.*, **90**, 1956 (2007).

Kuo, C. Y. and S. Y. Lu, "Fabrication of a Multi-Scale Nanostructure of TiO_2 for Application in Dye-Sensitized Solar Cells," *Nanotechnology*, **19**, 095705 (2008a).

Kuo, C. Y. and S. Y. Lu, "Opaline Metallic Photonic Crystals Possessing Complete Photonic Band-gaps in Optical Regime," *Appl. Phys. Lett.*, **92**, 121919 (2008b).

Kuo, C. Y., S. Y. Lu, S. Chen, M. Bernards, and S. Jiang, "Stop Band Shift Based Chemical Sensing with Three-dimensional Opal and Inverse Opal Structures," *Sens. Actuators B*, **124**, 452 (2007).

Li, M. and G. C. Wang, "In-situ Measurement of Thickness Dependence of Magnetoresistance and Magnetic Hysteresis Loops of Ultrathin Co Films on a SiO_2/Si(1 1 1) Substrate," *J. Magn. Magn. Mater.*, **217**, 199 (2000).

Liang, H. P., Y. G. Guo, J. S. Hu, C. F. Zhu, L. J. Wan, and C. L. Bai, "Ni–Pt Multilayered Nanowire Arrays with Enhanced Coercivity and High Remanence Ratio," *Inorg. Chem.*, **44**, 3013 (2005).

Liu, W., X. Z. Li, J. P. Liu, X. K. Sun, C. L. Chen, R. Skomski, D. K. Zhang, and D. J. Sellmyer, "Enhanced Coercivity in Thermally Processed (Nd,Dy) $(Fe,Co,Nb,B)_{5.5}$/α-Fe Nanoscale Multilayer Magnets," *J. Appl. Phys.*, **97**, 104308 (2005).

O'Barr, R., S. Y. Yamamoto, S. Schultz, X. H. Wu, and A. Scherer, "Fabrication and Characterization of Nanoscale Arrays of Nickel Columns," *J. Appl. Phys.*, **81**, 4730 (1997).

Ross, C. A., M. Hwang, M. Shima, H. I. Smith, M. Farhoud, T. A. Savas, W. Schwarzacher, J. Parrochon, W. Escoffier, H. N. Bertram, F. B. Humphrey, and M. Redjdal, "Magnetic Properties of Arrays of Electrodeposited Nanowires," *J. Magn. Magn. Mater.*, **249**, 200 (2002).

Schneider, M., H. Hoffmann, and J. Zweck, "Magnetic Switching of Single Vortex Permalloy Elements," *Appl. Phys. Lett.*, **79**, 3113 (2001).

Wang, Z. and S. H. Fan, "Optical Circulators in Two-dimensional Magneto-optical Photonic Crystals," *Opt. Express*, **30**, 1989 (2005).

Wassermann, E. F., M. Thielen, S. Kirsch, A. Pollmann, H. Weinforth, and A. Carl, "Fabrication of Large Scale Periodic Magnetic Nanostructures," *J. Appl. Phys.*, **83**, 1753 (1998).

Wegrowe, J. E., D. Kelly, A. Franck, S. E. Gilbert, and J. P. Ansermet, "Magnetoresistance of Ferromagnetic Nanowires," *Phys. Rev. Lett.*, **82**, 3681 (1999).

Wu, C. Z., P. Yin, X. Zhu, C. Z. OuYang, and Y. Xie, "Synthesis of Hematite (alpha-Fe_2O_3) Nanorods: Diameter-size and Shape Effects on their Applications in Magnetism, Lithium Ion Battery, and Gas Sensors," *J. Phys. Chem. B*, **110**, 17806 (2006).

Xi, H. W. and Y. M. Shi, "High Frequency Magnetization Rotation Induced by a dc Spin-polarized Current in Magnetic Nanostructures," *J. Appl. Phys.*, **96**, 1585 (2004).

Xu, Y. B., E. T. M. Kernohan, D. J. Freeland, A. Ercole, M. Tselepi, and J. A. C. Bland, "Evolution of the Ferromagnetic Phase of Ultrathin Fe Films Grown on GaAs(1 0 0)-4x6," *Phys. Rev. B*, **58**, 890 (1998).

Zhang, X. Y., G. H. Wen, Y. F. Chan, R. K. Zheng, X. X. Zhang, and N. Wang, "Fabrication and Magnetic Properties of Ultrathin Fe Nanowire Arrays," *Appl. Phys. Lett.*, **83**, 3341 (2003).

Zhao, Z. L., J. S. Chen, J. Ding, J. B. Yi, B. H. Liu, and J. P. Wang, "Fabrication and Microstructure of High Coercivity FePt Thin Films at 400 Degrees C," *Appl. Phys. Lett.*, **88**, 052503 (2006).

Zheng, M., L. Menon, H. Zeng, Y. Liu, S. Bandyopadhyay, R. D. Kirby, and D. J. Sellmyer, "Magnetic Properties of Ni Nanowires in Self-assembled Arrays," *Phys. Rev. B*, **62**, 12282 (2000).